Supplementary Information (SI) for RSC Advances.
This journal is © The Royal Society of Chemistry 2025

Supplementary Information

Diverse Rare Ginsenosides Derived from Ginsenoside Re in Aqueous Methanol Solution via Heterogeneous Catalysis and Identified by HPLC-MS

Yanyan Chang[a], Bing Li[a], Yusheng Xiao[a], Mengya Zhao[a], Yujiang Zhou[a], Huanxi Zhao[a]*, and Yang Xiu[a]*

[a]*Jilin Ginseng Academy, Changchun University of Chinese Medicine, Changchun 130117, P. R. China*

* Corresponding author, Jilin Ginseng Academy, Changchun University of Chinese Medicine, Changchun 130117, P. R. China.

E-mail address: phoenix8713@sina.com; xiuyang@ccucm.edu.cn

Table S1 Calibration curve, R^2 value, linear range, LOD, LOQ, and stability of the 9 authentic ginsenoside standards detected by the developed HPLC-MS method.

Ginsenoside	Calibration curve	R^2	Linear range (μg/mL)	LOD (μg/mL)	LOQ (μg/mL)	Stability RSD (n=7, %)
Re	y = 1785.30x + 3378.40	0.999	1.19-289.85	0.0312	0.102	2.08
20(S)-Rg2	y = 2137.12x + 1523.81	0.996	1.78-275.28	0.0401	0.1323	2.83
20(R)-Rg2	y = 2619.20x + 5807.03	0.994	1.96-269.65	0.0353	0.1164	2.16
20(S)-Rh1	y =1587.19x + 1699.32	0.993	1.49-297.05	0.0398	0.1303	3.45
20(R)-Rh1	y = 2756.82x + 2808.62	0.998	1.22-244.03	0.0521	0.1719	2.89
Rh4	y = 2288.62x + 5095.57	0.991	1.39-267.34	0.0712	0.2349	2.86
Rk3	y = 2765.20x + 1088.12	0.995	1.16-272.06	0.0653	0.2154	1.58
Rg6	y = 2124.42x + 2468.92	0.996	1.20-289.56	0.0313	0.1032	3.54
F4	y = 1863.20x + 1433.36	0.991	1.38-294.43	0.0736	0.2428	2.13

Table S2 Precision, repeatability, and recovery of the 9 authentic ginsenoside standards detected by the developed HPLC-MS method.

Ginsenoside	Intraday precision RSD (n=9, %)	Interday precision RSD (n=6, %)	Repeatability RSD (n=6, %)	Recovery (%) / RSD (n=3, %)		
				80 %	100 %	120 %
Re	2.19	1.67	1.14	100.29/2.31	101.94/1.93	99.54/2.24
20(S)-Rg2	2.07	2.60	2.18	103.61/2.45	101.99/1.44	97.36/2.12
20(R)-Rg2	1.53	2.65	1.97	101.13/1.42	96.55/2.27	101.23/1.89
20(S)-Rh1	3.05	2.12	3.63	98.35/1.69	101.50/1.77	99.65/2.28
20(R)-Rh1	2.95	2.23	3.29	97.89/1.71	102.02/1.95	98.62/1.67
Rh4	3.87	3.65	3.01	100.43/2.39	99.35/1.96	98.02/1.96
Rk3	3.97	2.28	0.67	101.56/1.48	103.28/1.56	100.74/1.29
Rg6	1.25	1.46	3.13	96.35/0.62	100.13/1.55	99.52/2.23
F4	1.83	2.84	1.47	99.24/1.99	101.06/2.01	100.56/2.05

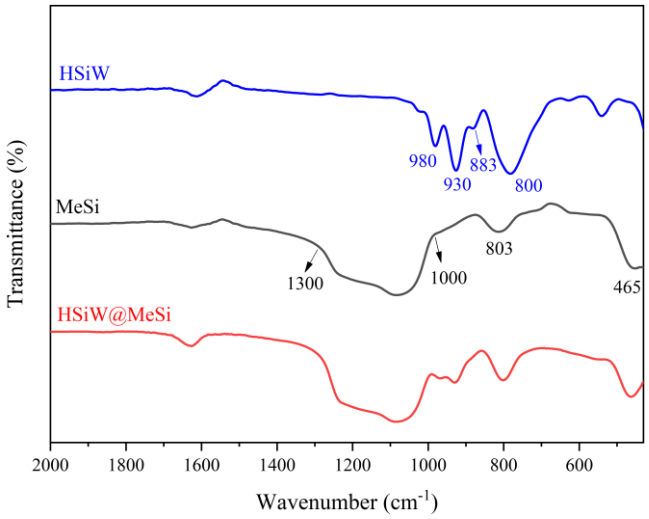

Fig. S1 FTIR spectra of HSiW, MeSi, and HSiW@MeSi.

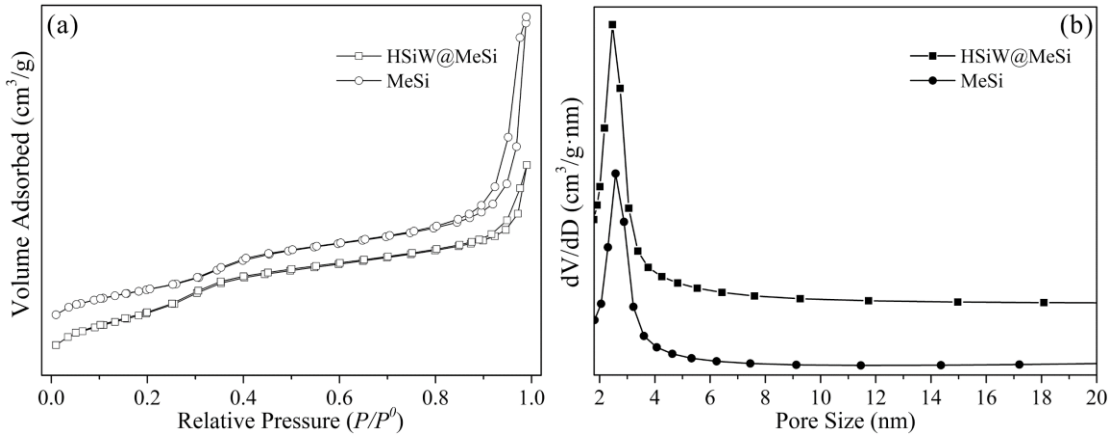

Fig.S2 N_2 adsorption-desorption isotherms (a) and pore size distributions (b) of MeSi and HSiW@MeSi.

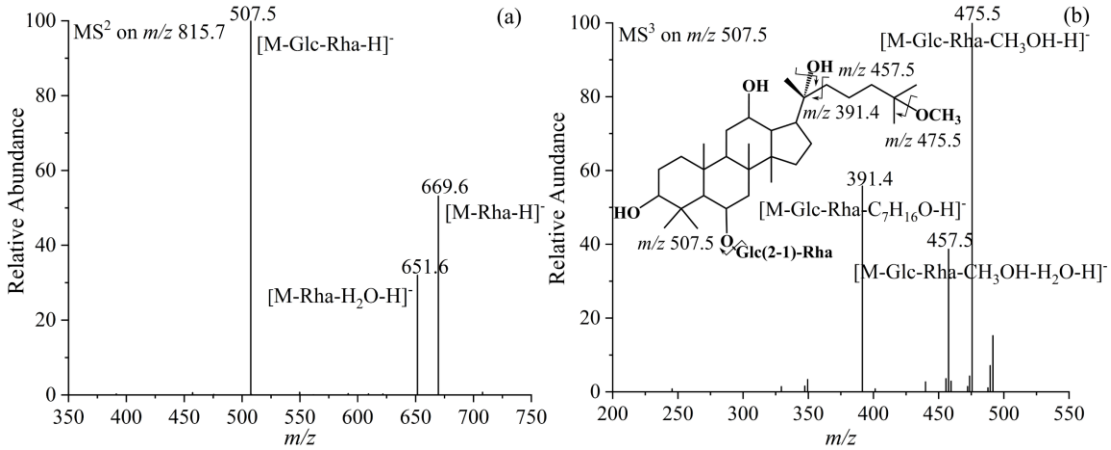

Fig. S3 MS^2 spectrum of the $[M-H]^-$ ion at *m/z* 815.7 (a), fragmentation pathways, and MS^3 spectrum of the product ion at *m/z* 507.5 (b) from ginsenoside 20(R)-25-OCH_3-Rg2.

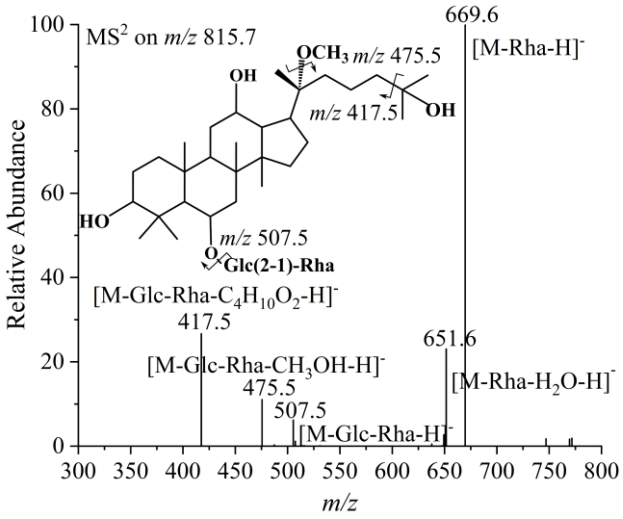

Fig. S4 MS^2 spectra of the ion at *m/z* 815.7 the $[M-H]^-$ ion of ginsenoside 20(R)-OCH_3-25-OH-Rg2.

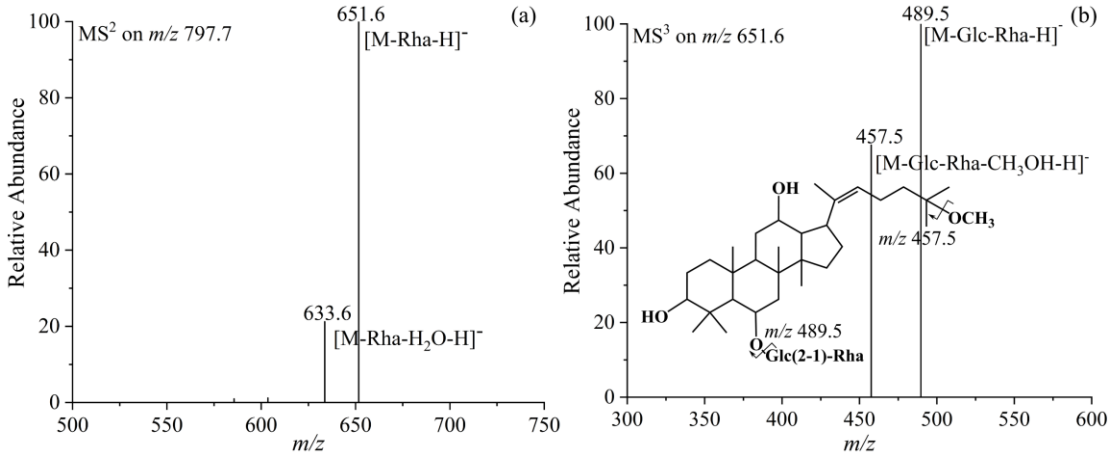

Fig. S5 MS^2 spectrum of the $[M-H]^-$ ion at *m/z* 797.7 (a), fragmentation pathways, and MS^3 spectrum of the product ion at *m/z* 651.6 (b) from ginsenoside 25-OCH_3-F4.

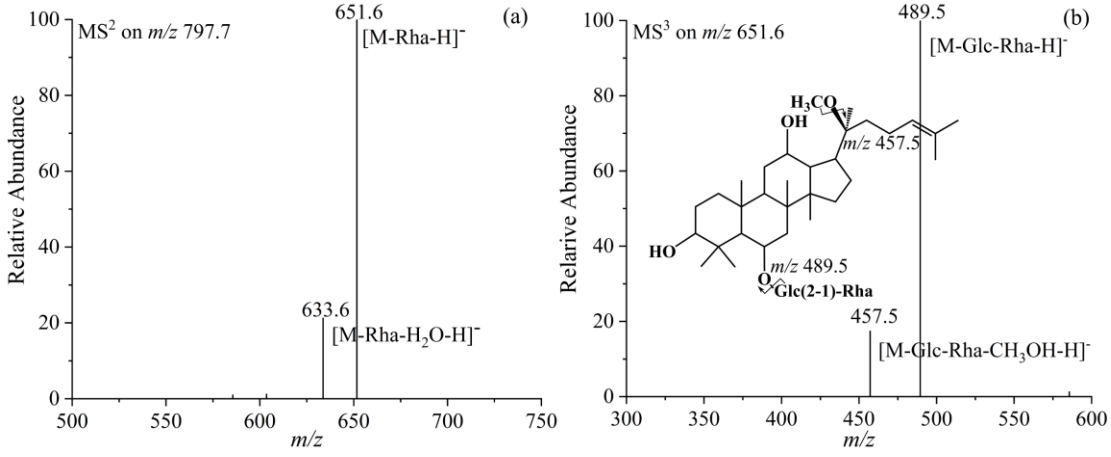

Fig. S6 MS^2 spectrum of the $[M-H]^-$ ion at *m/z* 797.7 (a), fragmentation pathways, and MS^3 spectrum of the product ion at *m/z* 651.6 (b) from ginsenoside 20(S)-OCH_3-Rg2.

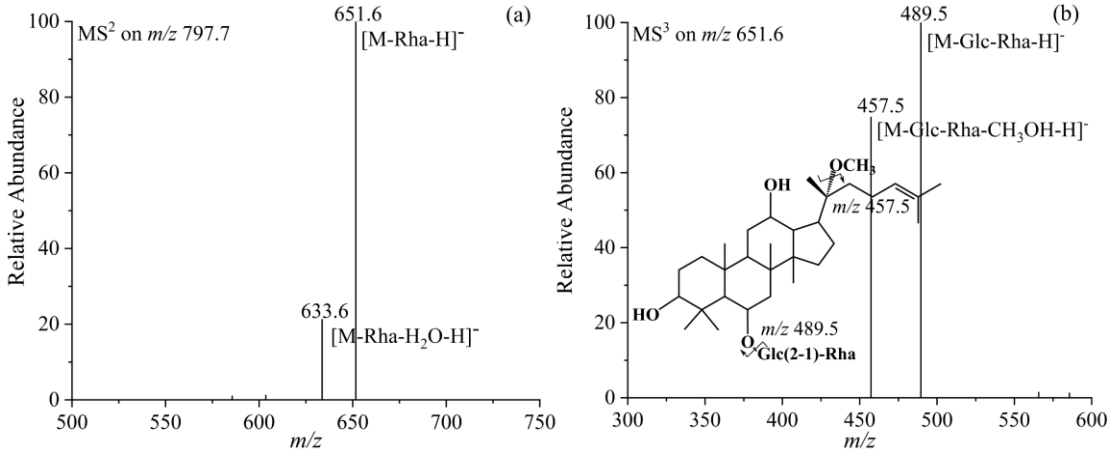

Fig. S7 MS^2 spectrum of the $[M-H]^-$ ion at *m/z* 797.7 (a), fragmentation pathways, and MS^3 spectrum of the product ion at *m/z* 651.6 (b) from ginsenoside 20(R)-OCH_3-Rg2.

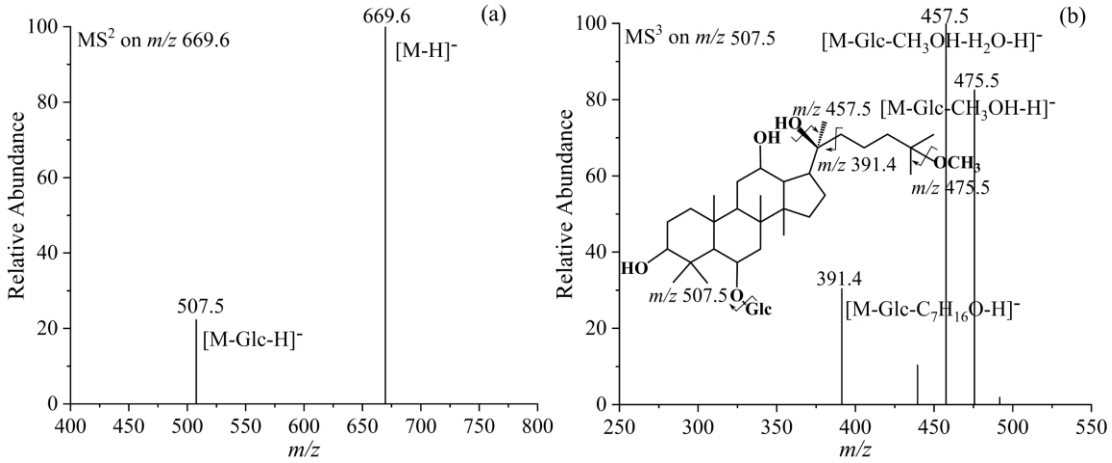

Fig. S8 MS^2 spectrum of the $[M-H]^-$ ion at *m/z* 669.6 (a), fragmentation pathways, and MS^3 spectrum of the product ion at *m/z* 507.5 (b) from ginsenoside 20(S)-25-OCH_3-Rh1.

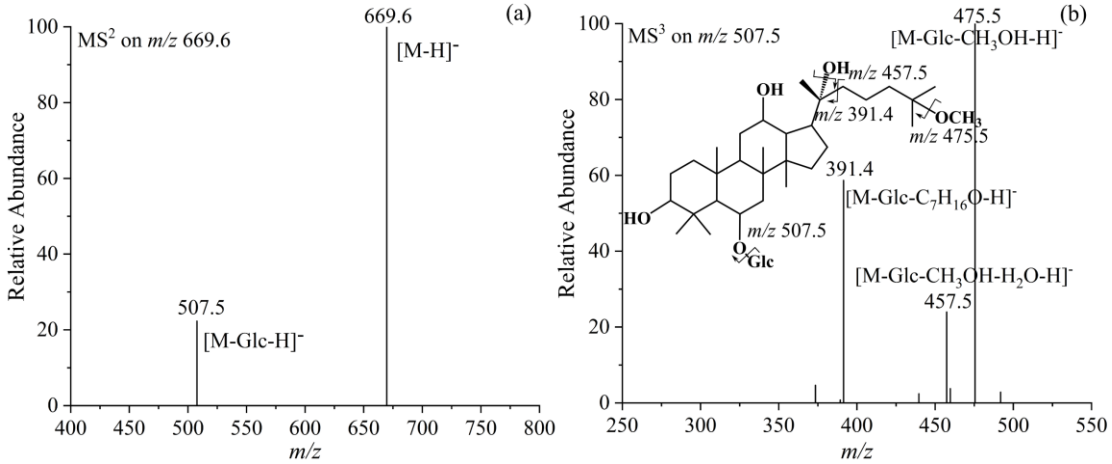

Fig. S9 MS^2 spectrum of the $[M-H]^-$ ion at *m/z* 669.6 (a), fragmentation pathways, and MS^3 spectrum of the product ion at *m/z* 507.5 (b) from ginsenoside 20(R)-25-OCH_3-Rh1.

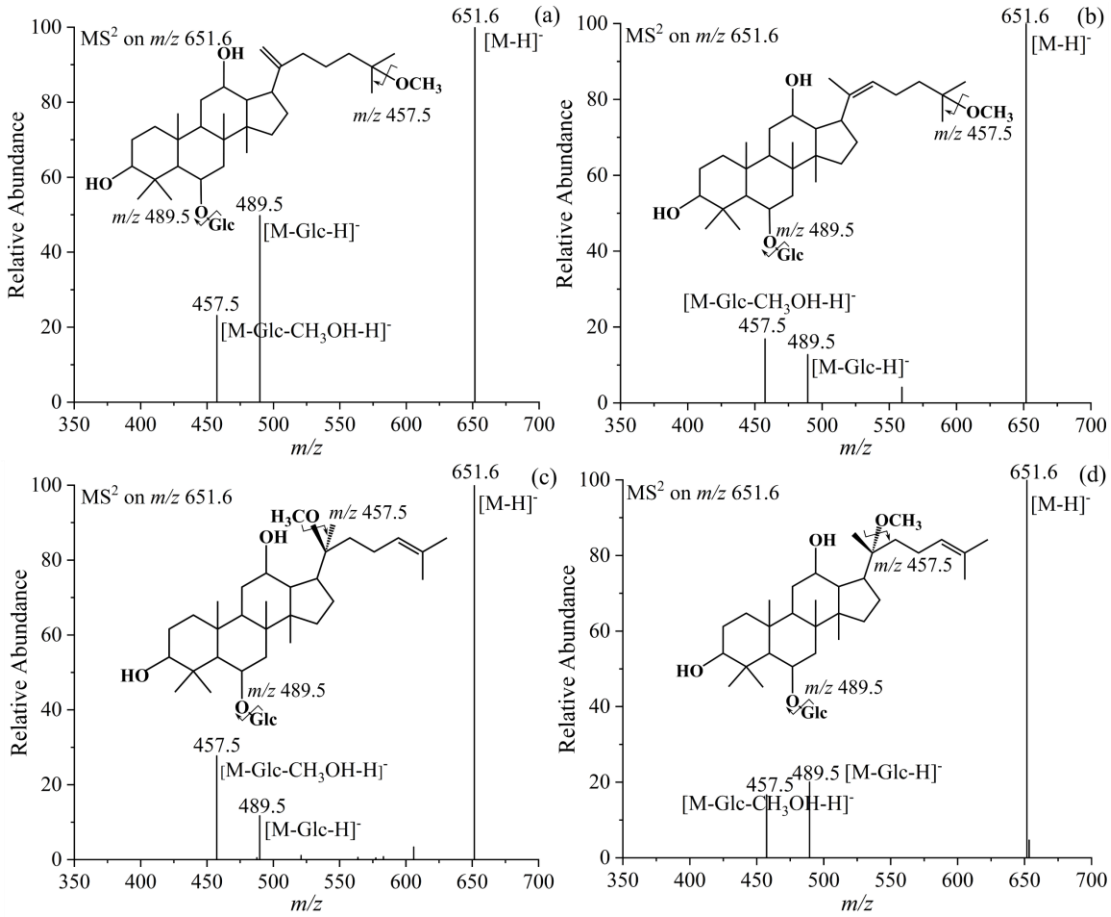

Fig. S10 MS^2 spectra of the ion at m/z 651.6 the [M-H]- ion of ginsenoside25-OCH3-Rk3 (a), 25-OCH3-Rh4 (b), 20(S)-OCH3-Rh1 (c), and 20(R)-OCH3-Rh1 (d).

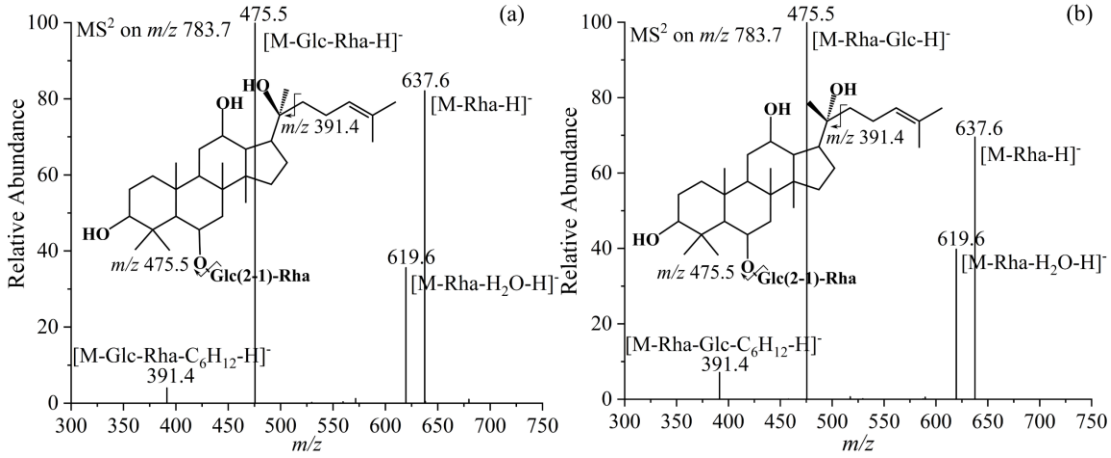

Fig. S11 MS^2 spectra of the ion at *m/z* 783.7 the $[M-H]^-$ ion of ginsenoside 20(S)-Rg2 (a) and 20(R)-Rg2 (b).

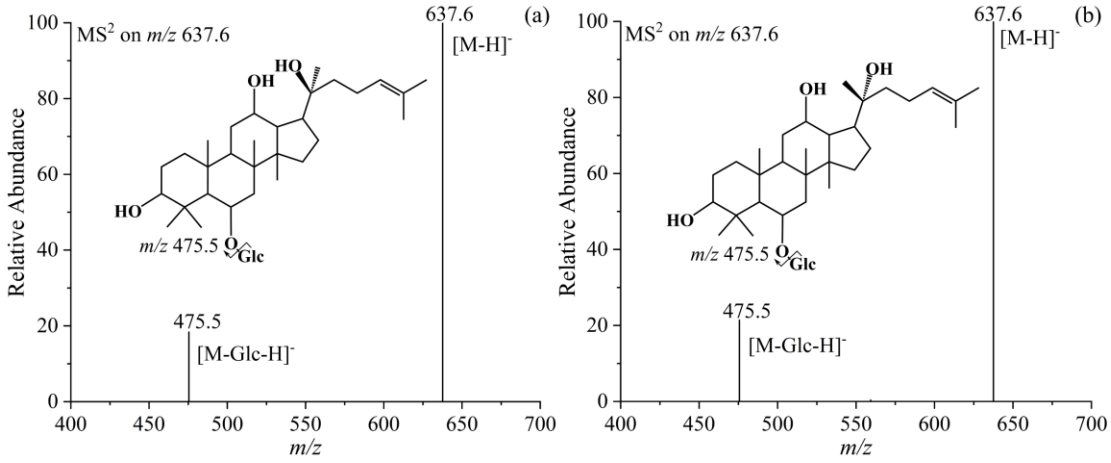

Fig. S12 MS^2 spectra of the ion at *m/z* 637.6 the $[M-H]^-$ ion of ginsenoside 20(S)-Rh1 (a) and 20(R)-Rh1 (b).

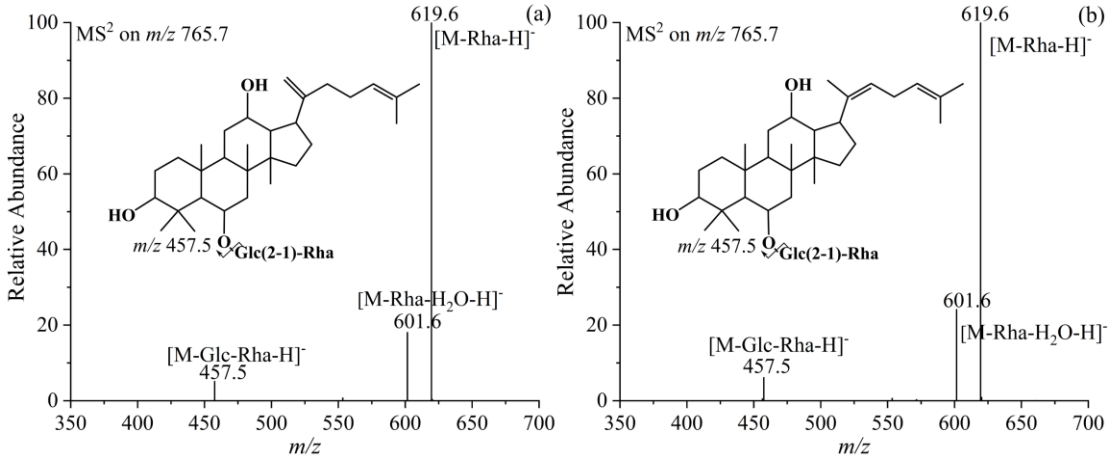

Fig. S13 MS^2 spectra of the ion at *m/z* 765.7 the $[M-H]^-$ ion of ginsenoside Rg6 (a) and F4 (b).

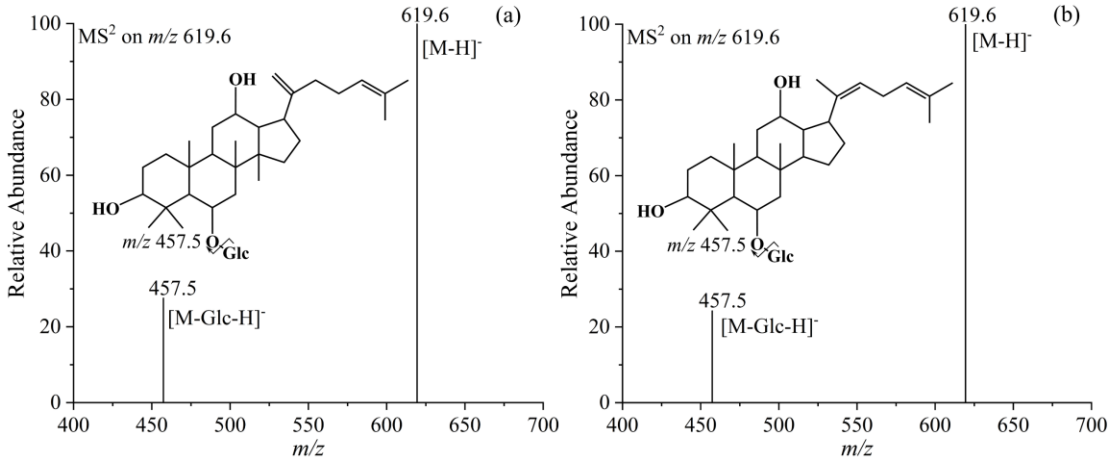

Fig. S14 MS^2 spectra of the ion at *m/z* 619.6 the $[M-H]^-$ ion of ginsenoside Rk3 (a) and Rh4 (b).

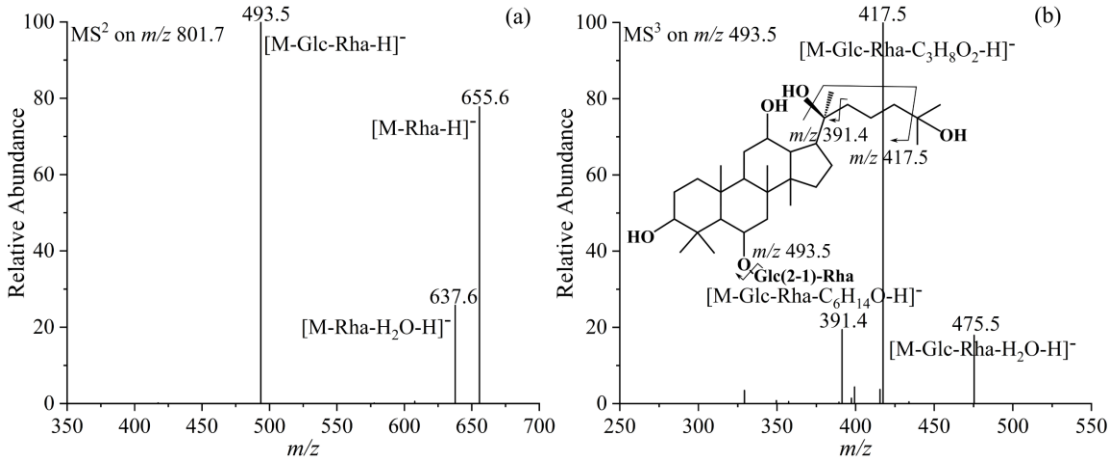

Fig. S15 MS^2 spectrum of the [M-H]- ion at m/z 801.7 (a), fragmentation pathways, and MS^3 spectrum of the product ion at m/z 493.5 (b) from ginsenoside 20(S)- Rf2.

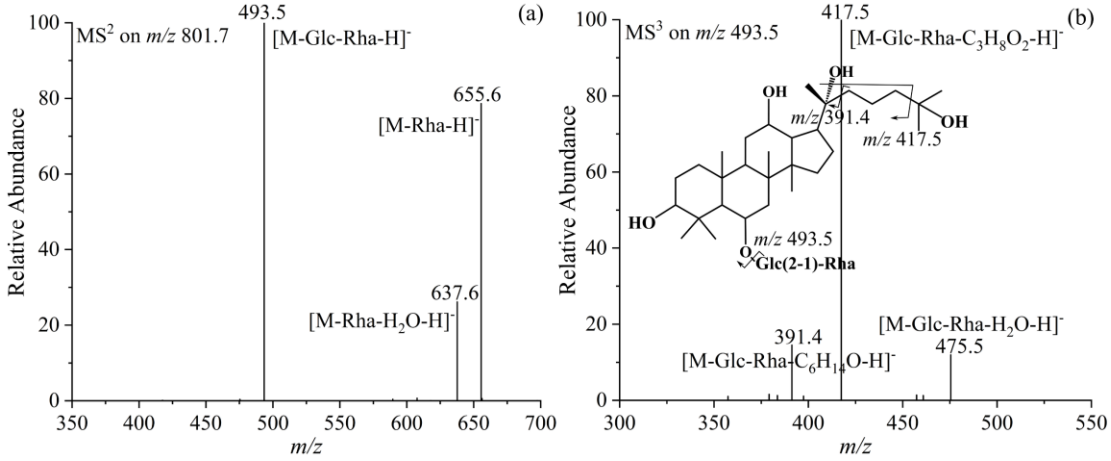

Fig. S16 MS^2 spectrum of the [M-H]- ion at m/z 801.7 (a), fragmentation pathways, and MS^3 spectrum of the product ion at m/z 493.5 (b) from ginsenoside 20(R)- Rf2.

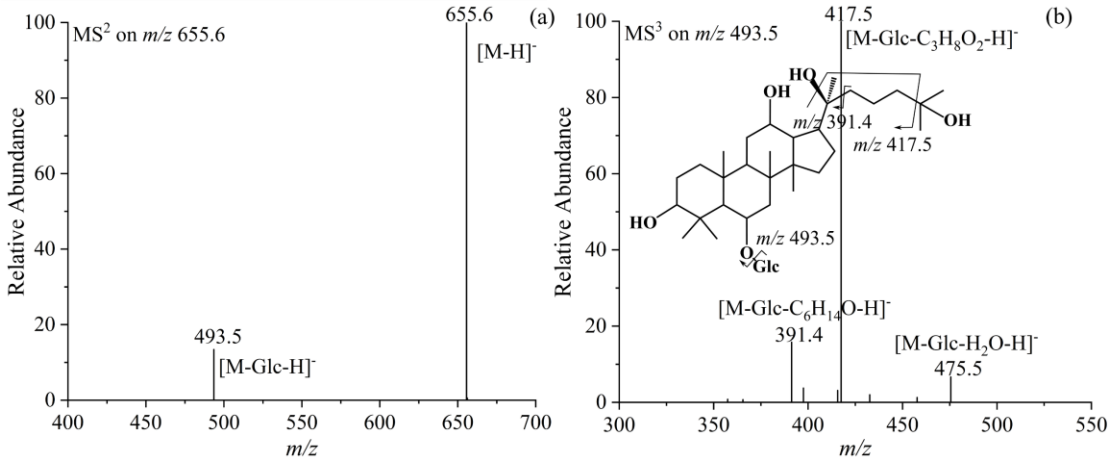

Fig. S17. MS^2 spectrum of the [M-H]- ion at m/z 655.6 (A), fragmentation pathways, and MS^3 spectrum of the product ion at m/z 493.5 (B) from ginsenoside 20(S)-25-OH-Rh1.

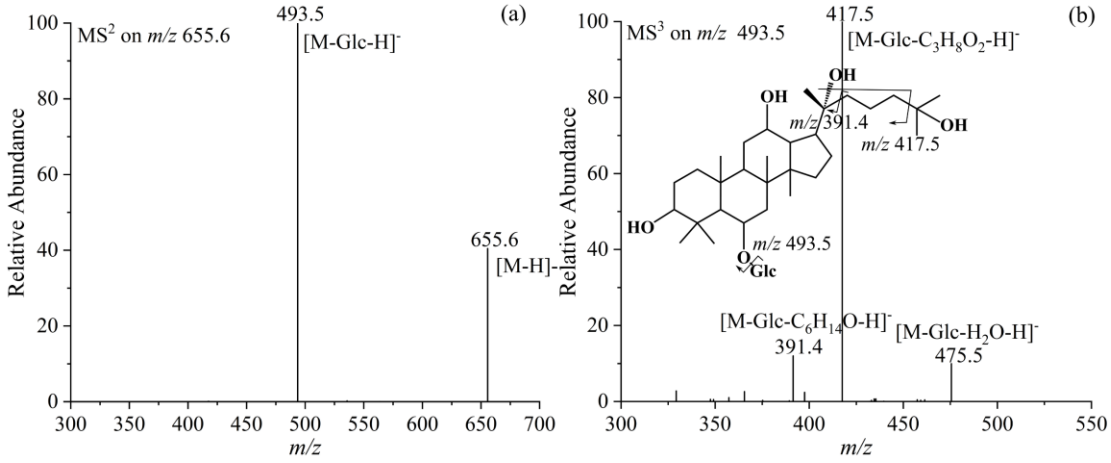

Fig. S18 MS^2 spectrum of the [M-H]- ion at m/z 655.6 (a), fragmentation pathways, and MS^3 spectrum of the product ion at m/z 493.5 (b) from ginsenoside 20(R)-25-OH-Rh1.

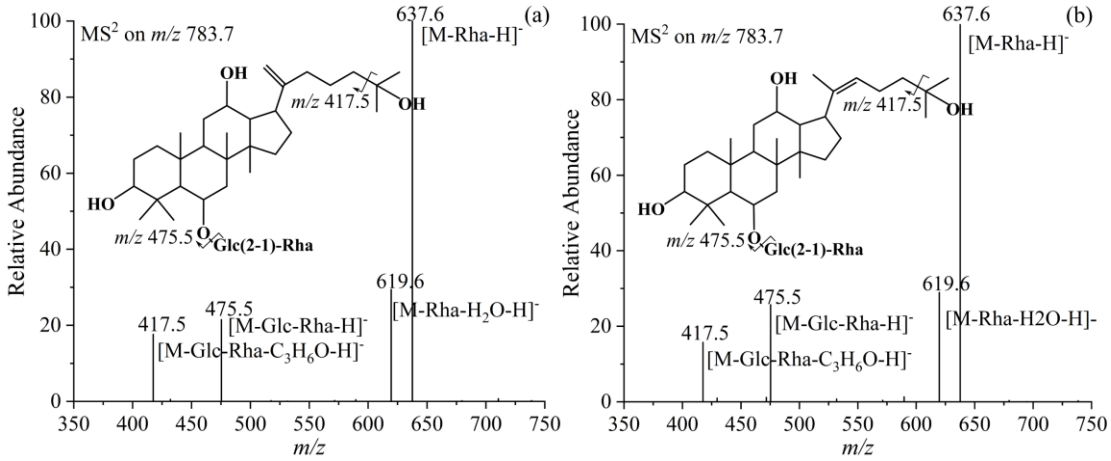

Fig. S19 MS^2 spectra of the ion at *m/z* 783.7 the $[M-H]^-$ ion of ginsenoside 25-OH-Rg6 (a) and 25-OH-F4 (b).

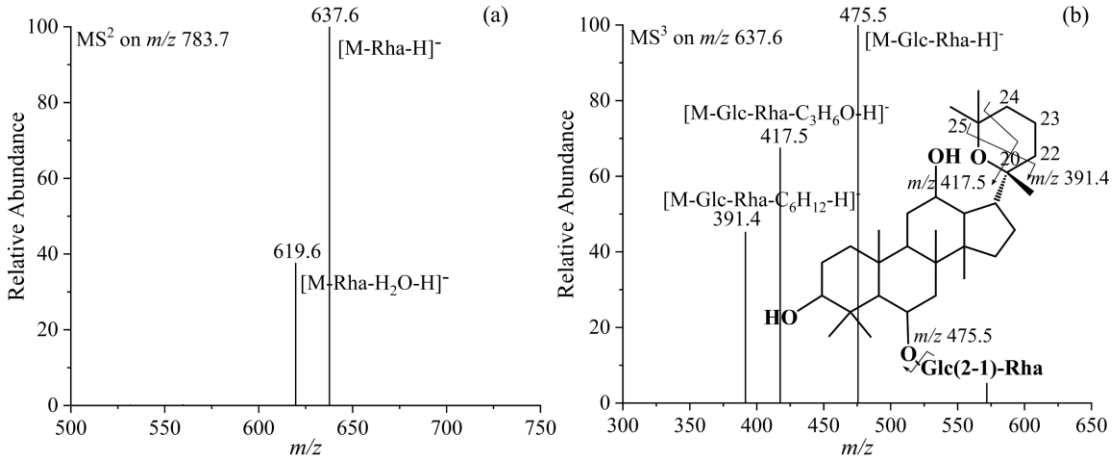

Fig. S20 MS^2 spectrum of the $[M-H]^-$ ion at *m/z* 783.7 (a), fragmentation pathways, and MS^3 spectrum of the product ion at *m/z* 637.6 (b) from ginsenoside 20(R,25)-epoxy-Rg2.